CryoEM PSII structure reveals adaptation mechanisms to environmental stress in *Chlorella ohadii*

Maria Fadeeva*, Daniel Klaiman*, Ido Caspy, and Nathan Nelson**

Department of Biochemistry and Molecular Biology, The George S. Wise Faculty of Life Sciences, Tel Aviv University, 69978 Tel Aviv, Israel

*Equally contributed

** To whom correspondence should be addressed:

nelson@tauex.tau.ac.il

Summary

Performing photosynthesis in the desert is a challenging task since it requires a fast adaptation to extreme illumination and temperature changes. To understand adaptive mechanisms, we purified Photosystem II (PSII) from *Chlorella ohadii*, a green alga from the desert soil surface, and identified structural elements that might enable the photosystem functioning under harsh conditions. The 2.72 Å cryogenic electron-microscopy (cryoEM) structure of PSII exhibited 64 subunits, encompassing 386 chlorophylls, 86 carotenoids, four plastoquinones, and several structural lipids. At the luminal side of PSII, the oxygen evolving complex was protected by a unique subunit arrangement - PsbO (OEE1), PsbP (OEE2), CP47, and PsbU (plant OEE3 homolog). PsbU interacted with PsbO, CP43, and PsbP, thus stabilising the oxygen evolving shield. Substantial changes were observed on the stromal electron acceptor side - PsbY was identified as a transmembrane helix situated alongside PsbF and PsbE enclosing cytochrome b559, supported by the adjacent C-terminal helix of Psb10. These four transmembrane helices bundled jointly, shielding cytochrome b559 from the solvent. The bulk of Psb10 formed a cap protecting the quinone site and probably contributed to the PSII stacking. So far, the *C. ohadii* PSII structure is the most complete description of the complex, suggesting numerous future experiments. A protective mechanism that prevented Q_B from rendering itself fully reduced is proposed.

Main

Oxygenic photosynthesis of cyanobacteria, various algae, and land plants converts light energy from the sun into a biologically useful chemical energy concomitant, with the evolution of molecular oxygen[1,2]. The light reactions of photosynthesis depend on the functions of photosystem II (PSII), cytochrome b6f, and photosystem I (PSI). Driven by photon energy, these membrane-embedded machineries carry out a linear electron transfer from water to NADP+, and eventually, reduce CO_2 to form organic material[3]. PSI exhibits a different structural organisation among the photosynthetic organisms, while PSII organises itself mainly into a dimer, regardless of the species

of the organism. However, PSII interacts with a variety of light-harvesting proteins, to form supercomplexes of different sizes and shapes[4]. In *Chlamydomonas reinhardtii*, the various supercomplexes include C2S2 and C2S2M2L2 (C indicates the PSII core, while S, M, and L indicate strongly, moderately, and loosely associated LHCII, respectively). Among these, C2S2M2L2 is the largest known PSII–LHCII supercomplex in green algae or plants [4,5]. So far, none of the published structures of PSII contains all the expected subunits of the complex. Performing photosynthesis under extreme high light (HL) intensities is a challenge for the photosynthetic organisms, as well as for the artificial systems that rely on natural photosystems. As such, specialised photoautotrophs have devised mechanisms to dissipate the excess excitation energy, and reduce the potential photodamage that intense illumination causes to PSII, and also to the less sensitive Photosystem I (PSI)[6,7]. The green alga *Chlorella ohadii*, which was isolated from a desert biological soil crust, copes with these harsh conditions, including extremely high daytime illumination (~2000 μE)[8]. Unlike other photosynthetic organisms, *C. ohadii* does not undergo photodamage, even when exposed to light intensities that are 3 to 4-fold higher than that which is required to saturate the CO_2 fixation[9]. It has been proposed that under high illumination, *C. ohadii* activates several protection mechanisms, including a massive cyclic electron transport within PSII that can be as high as 90% of the electrons from water splitting[10,11]. These adaptive capabilities should be reflected in structural alterations in the PSII complex. We isolated a highly active PSII supercomplex from *C. ohadii* and determined its high-resolution structure (Fig. 1, Fig. S1 and 2) using cryoEM (Methods). Overall, the structure resembled that of the C2S2M2L(N)2-type PSII-LHCII supercomplex from *C. reinhardtii* (PDBID 6KAD and 6KAF)[4,12]. Our new structure contains three additional subunits in each PSII monomer, denoted as PsbP, Psb10, and PsbY (Fig. 1 and 2), which might serve as pillars for the stability of the *C. ohadii* complex (PDBID 8BD3). Moreover, subunits that are critical for the stability and the oxygen evolution of PSII are better resolved, exhibiting critical interaction sites with other subunits of the complex. The cryoEM

63 structure of PSII at 2.72 Å unveiled 64 subunits containing 386 chlorophylls, 86 carotenoids, four
64 plastoquinones, and several conserved structural lipids.

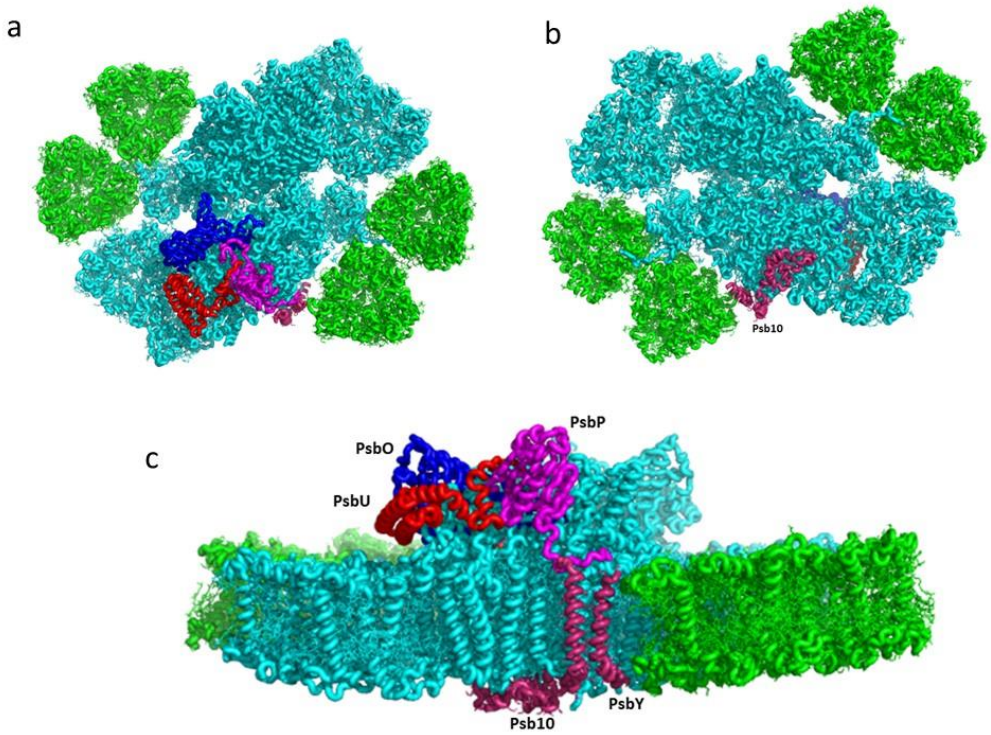

65

66 **Figure 1: CryoEM structure of the *C. ohadii PSII* complex*:***
67 **a**) Top view of the supercomplex from the stromal side. The novel or rare subunits are coloured
68 (PsbP-magenta, PsbO-blue, PsbU-red, and Psb10 and PsbY are in purple. **b**) Luminal view of
69 the supercomplex. **c**) Side view along the membrane plane.
70

71 PSII reaction centre is engulfed by shielding subunits, both from the luminal and stromal side (Fig.
72 2 and 3). The function of these extrinsic luminal subunits of PSII is still under strong debate [13-15].
73 In higher plants, they have been proposed to operate primarily during the biogenesis of the
74 complex[14]. The main conclusion from the numerous reported experiments is that these domains
75 are essential for the stability of the PSII supercomplex. The structure of the luminal extrinsic
76 subunits and their interactions have been elucidated (Fig. 3). It is well documented that Oxygen
77 Enhancer Element 1 PsbO (OEE1) intactness is critical for the stability and the activity of PSII. A
78 single amino acid substitution (P104H) in *C. reinhardtii* has rendered PSII temperature sensitive
79 and caused the disappearance of the entire complex at the nonpermissive temperature of 37°C[16].

The tertiary structure of *C. ohadii* PsbO is quite conserved, albeit sharing just 75% identity with the sequence of the *C. reinhardtii* protein. *C. ohadii* PsbO is secured by strong interactions with CP47 via a stabilising loop that was not resolved in the *C. reinhardtii* structure, together with subunit PsbP, that is not present in the latter structures (PDBID 6KAD and 6KAF) [4,12].

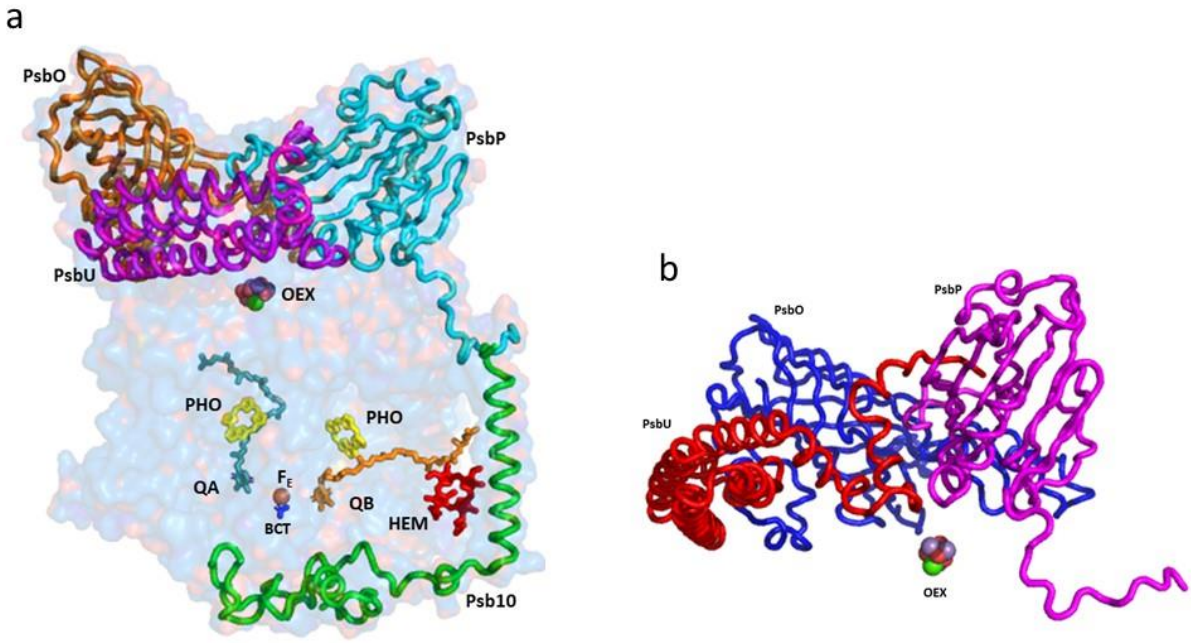

Figure 2: Side view of the subunits that are shielding the reaction centre:
a) The indicated subunits and the prosthetic groups are shown on the background of a surface model, with 80% transparency of the PsbA, PsbB, PsbC, PsbD, PsbP, PsbO, PsbU, and Psb10 subunits. **b**) The structure of the luminal extrinsic subunits and their interactions with each other: A ribbon presentation of the three main subunits protecting the oxygen evolving complex (OEX). The extensive interactions among OEE1 (PsbO), OEE2 (PsbP), and OEE3 (PsbU) are shown.

PsbP is an Oxygen Enhancer Element 2 (OEE2) that was pronouncedly present in our structure (Fig. 1 and 2). PsbP deletion in *C. reinhardtii* resulted in the loss of oxygen evolution activity but was only marginally affected the assembly of the other PSII subunits[17]. Regardless of its expression in the various organisms, PsbP was missing in several of the PSII preparations. In *C. reinhardtii*, PSII was identified in the cryoEM structure of the C2S2-type PSII-LHCII supercomplex from (PDB 6KAC)[4], however, it was not present in the structure of the larger PSII

form (PDB 6KAD)[12]. The *C. ohadii* PsbP counterpart was only 69% identical to its *C. reinhardtii* homologue. Yet, despite the differences in the amino acid sequences, the structure of the corresponding subunits was relatively similar. Thus, the interaction between the specific amino acids was probably responsible for the stability that *C. ohadii* OEE2 conferred. One example is a R368F substitution 16 Å away of the oxygen evolving complex (OEC). A nearby substitution of K371G might also contribute to the stability of this important site. The tight binding of PsbP might contribute to the overall stability of the large luminal structure that protects OEC.

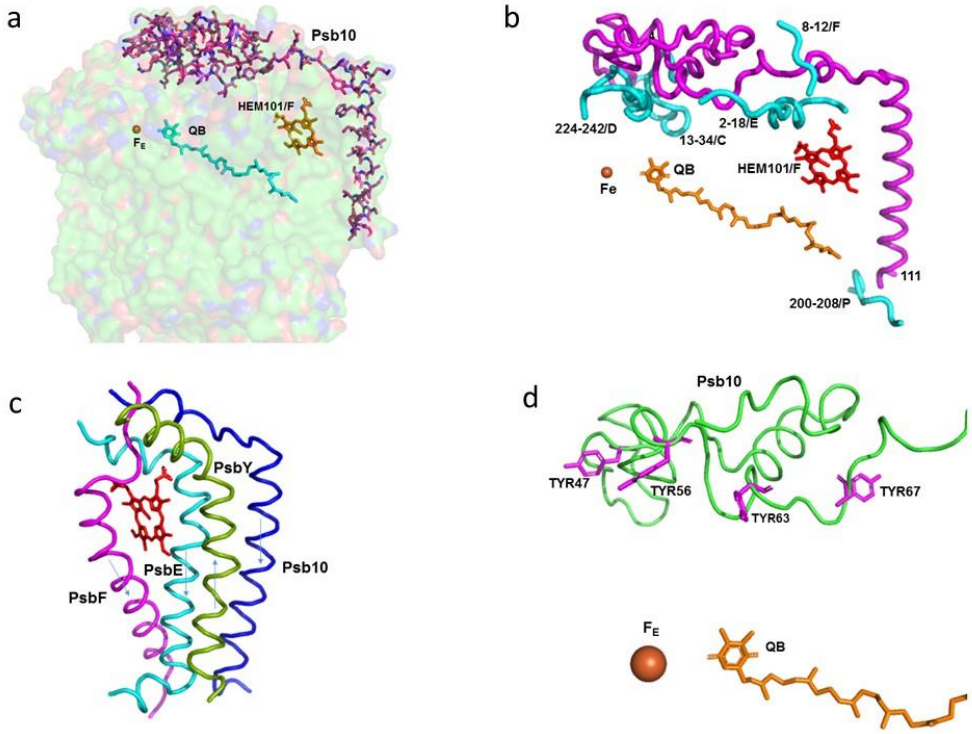

Figure 3: The structure and interaction of the subunits involved in the protection of the acceptor site of PSII, including Fe, Q_B, and cytochrome b559:
a) Stick presentation of Psb10 shown on the background of a surface model, with 80% transparency of the subunits PsbA, PsbC, PsbD, PsbE, PsbF, PsbY, and Psb10. **b**) Interaction of Psb10 with the various PSII subunits: A ribbon presentation of the Psb10 interaction with the indicated subunits. **c**) Transmembrane helices shielding the heme of cytochrome b559. The transmembrane helices of Psb10, PsbE, and PsbF are going from the stroma to the lumen. The helix of PsbY is going in the opposite direction. **d**) Four tyrosine residues of Psb10 pointing to the Fe-Q_B location.

The sequence of the nuclear gene of the 16 kDa Oxygen Enhancer Element 3 (OEE3) polypeptides present in the oxygen evolving complex of *C. reinhardtii* have been established[18,19]. The comparison between the OEE3 protein sequences of *C. reinhardtii* and the higher plants has revealed a mere 28% overall homology, mostly limited to the central portion of the protein. We identified OEE3 in the *C. ohadii* PSII structure (PsbU) as four bundled helices laying atop CP43, contacting PsbO (Fig. 2). PsbU extended N-terminus contacted with PsbP, supported by a subsequent helix-helix interaction with CP43 (Fig. 2). This arrangement has suggested a major function in stabilising the entire large complex, isolating the OEC from the luminal medium. The PsbU subunit, like PsbP, was absent in the large PSII complex from *C. reinhardtii* (PDBID 6KAD).

Due to the formation of stacked PSII in the grana, there was no place for large protrusions at the stromal side of the complex. So far, no specific amino acid sequences were shown to be directly involved in the PSII dependent grana formation[20]. The structure of *C. ohadii* PSII presented a slight deviation of this rule by the presence of the "PSII 10 kDa polypeptide". This subunit has been denoted as Psb10 and was evident in our structure (Fig. 2-3). An unidentified stromal protein (USP) that was present in the C2S2 supercomplex but was not observed in the C2S2M2L2 supercomplex of *C. reinhardtii* might be its homologue[4]. Subunit Psb10 was located at the interface between two adjacent C2S2 supercomplexes that are stacked with each other along their stromal surface and might represent the partial Psb10 subunit that is entirely present in the *C. ohadii* structure (Fig. 3). According to the published sequences, Psb10 was not present only in algae but also in moss and higher plants - but not in cyanobacteria. This suggests that Psb10 might have immerged alongside the PSII mediated grana staking. The Psb10 polypeptide N-terminus was located at the stroma, forming a cap over the interface between CP43 and D2, subsequently, establishing an interface with PsbE and PsaF N-termini. Finally, it formed a transmembrane helix parallel to and in a strong contact with PsbE transmembrane helix (Fig. 3). The position of this helix was similar to that of the alpha helix that was identified in PDB 6KAC and built as a

polyalanine chain[4]. The Psb10 C-terminus interacted with PsbP on the luminal side of the membrane (Fig. 2 and 3). This arrangement leaves little doubt regarding the important function of Psb10 in stabilising the *C. ohadii* PSII supercomplex. Finally, Psb10 might support the interaction between the two PSII complexes that form the stacked PSII (Fig. S3). The function of Psb10 is unknown but its four tyrosine residues facing the Q_A-Fe-Q_B cluster suggest an involvement in protection against radicals (Fig. 2-4).

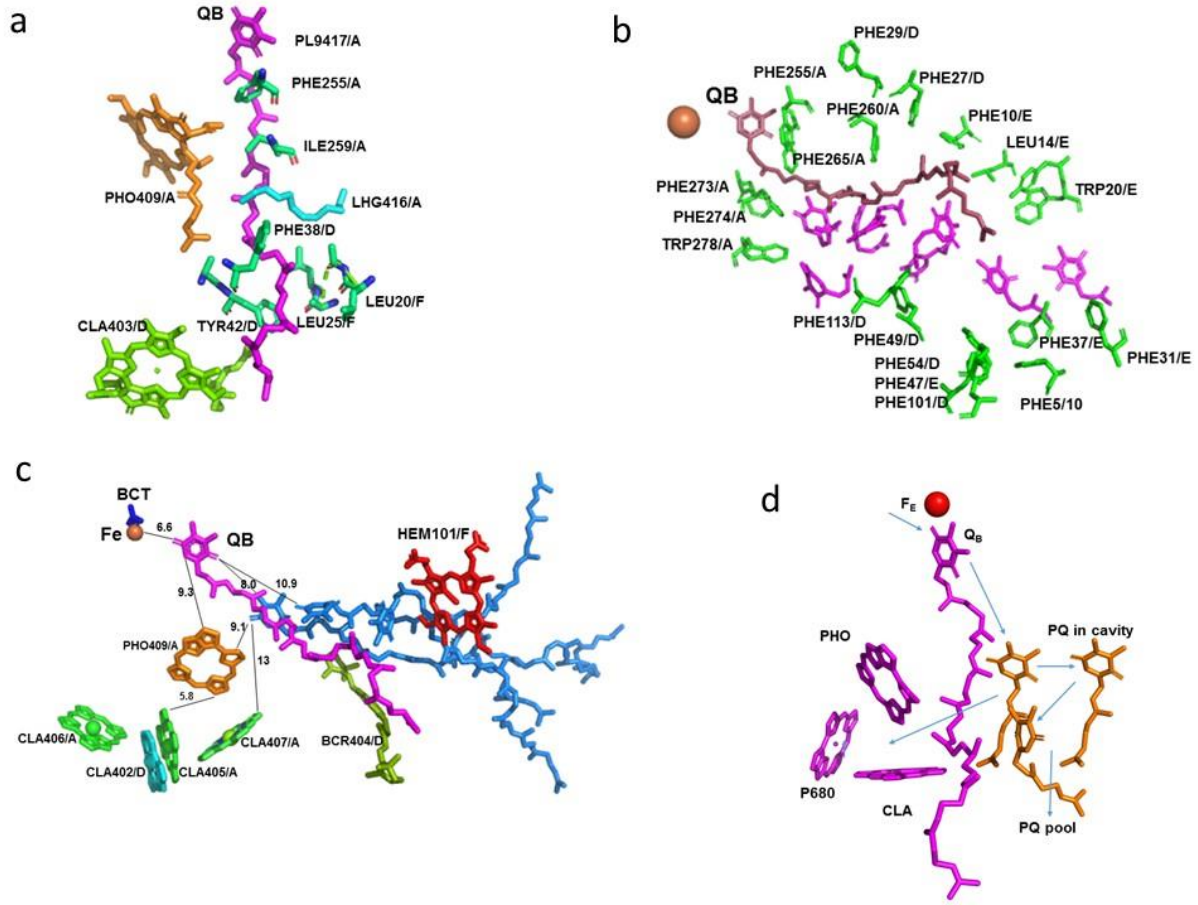

Figure 4: Structure of Q_B and its vicinity in relation to the factors involved in the electron transport and quenching:
a) Interactions of Q_B with the surrounding amino acids and prosthetic groups. The amino acids and the prosthetic groups that are in contact with Q_B are specified. **b**) Hydrophobic cavity proceeding from Q_B to the exterior of the complex. The amino acids surrounding the cavity are specified and coloured green. Space filling of seven Q1 molecules (magenta) modelled into the cavity with no structural clashes. **c**) Position and distances of the prosthetic groups pertinent for the function of PSII. Three plastoquinone molecules (light blue) modelled into the cavity with no structural clashes. The indicated distances are in Å. **d**) Potential electron transfer pathways

158 that might involve in the electron transfer from Q_B to plastocyanin, quenching, and the cyclic
159 electron transport.
160

161 Another pillar connected to the subunits PsbE, PsbF, and Psb10 was the position of PsbY in the
162 PSII complex. PsbY is a single transmembrane helix protein, yet it is encoded and translated as
163 multiple copies in a single protein. In *C. ohadii*, PsbY appeared in four copies, but in some green
164 algal species, such as *Micractinium conductrix, Volvox, Chlamydomonas,* and *Scenedesmus*, it
165 manifested itself in 3-5 copies, while in the higher plants, only two copies were present in a single
166 transcript. The copies within the transcript were identical, or highly homologous. Polyprotein
167 transcripts are quite common in viruses[21], and it would be of no surprise if PsbY is of viral origin.
168 This notion was supported by the different copies present in the closely related organisms (Fig.
169 S4).

170 PsbY joined a triplet of transmembrane helices that were formed by PsbE, PsbF, and Psb10, while
171 running antiparallel to them (Fig. 3c). Together, they shield the heme group of cytochrome b559,
172 which otherwise would be exposed to the membrane interior environment. This arrangement also
173 stabilised the position of the prosthetic group that might be crucial for the protection of PSII from
174 photodamage caused by excessive light intensities, when electron acceptors are lacking.

175 Following light absorption, charge separation converts excited P680* to create the longer-lived
176 state $Yz^+ Q_A^-$. The hole in Yz^+ can be filled by an electron from the manganese oxygen evolving
177 complex (OEC), or from the electron acceptor side, either directly, or via rapid equilibrium with
178 $P680^+$. Under ambient conditions, Q_A^- transfers its electron forward to Q_B, which is mediated by
179 the non-heme iron site[22]. The reaction is relatively slow, and takes place in a sub millisecond time
180 range[23]. If the oxidized quinones are absent, or present in limited availability, the electron may
181 return via many possible routes to $P680^+$ or OEC. None of these routes are visible under continuous
182 light, or even via the S-state turnover measurements[24-26] and it was considered as radical protective

cyclic electron transport[25-27]. Cytochrome b559 was suggested to participate in this cyclic electron transport [28]. The presence of oxidized PQ in tiny amounts, which was maintained by the cycling electrons, might be sufficient to protect this photosynthetic organism from radical damage.

The efficient drainage of electrons/reductants from the reaction centres for metabolic or other uses could help protect the photosynthetic machinery from the damage that is caused by the excess illumination[10]. Q_A•-, the reduced semiquinone form of the nonexchangeable quinone, is often considered capable of a side reaction with O_2, forming superoxide and damaging radicals[27,28]. Fantuzzi et al., (2022)[29], using chlorophyll fluorescence in plant PSII membranes, showed that O_2 oxidizes $Q_A^{\bullet-}$ at physiological O_2 concentrations, with a $t_{1/2}$ of 10 s. $Q_A^{\bullet-}$ could only reduce O_2 when bicarbonate was absent from its binding site on the nonheme iron (Fe^{2+}). It was concluded that the reduction of O_2 was favourable when the oxygen binds directly to Fe^{2+}. This contrasts with a previously proposed mechanism involving direct oxidation of Q_A•- by O_2, which was expected to require close contact between the oxygen and the semiquinone[29-32]. Thus, *C. ohadii* PSII, which copes with extreme high daytime illumination of up to 2000 µE, either contains an extremely tight bicarbonate binding site, or has an altered sequence of events that are linked to the reduction state of the quinone pool[33]. Our structure suggests a conserved bicarbonate binding site. However, in contrast to most preparations of PSII, where Q_B is missing, in *C. ohadii* Q_B, it was clearly identified at its binding site. This structure revealed strong interactions with the surrounding amino acids and prosthetic groups (Fig. 4a). It is worth noting that the terminal end of its isoprenoid chain was tightly held by the surrounding hydrophobic amino acids. We propose that the tight binding of Q_B and the plastoquinones in the hydrophobic pocket are responsible for the PSII resistance to the high light intensities. Accordingly, the direct electron transfer from Q_A^- to Q_B and the fast transfer of the electron from Q_B^- to the quinone pool protects *C. ohadii* PSII from photodamage. The observation that the plastoquinone pool of *Nannochloropsis oceanica* was not completely reduced during the bright light pulses[34], as well as in the plants[35], is in line with this study's proposal for

the mechanism of photoprotection in *C. ohadii*. A wide hydrophobic cavity was observed, starting at Q_B and going out of PSII to the middle of the membrane, and might contain several quinones (Fig. 5). A similar cavity was detected in the crystal structure of *T. elongatus,* and it was proposed to harbour a specialised quinone Q_C[35-38]. The potential occupancy allowed the quinones to pack together, maintaining distances of less than 10 Å from each other (Fig. 4c). This distance allowes electron transfer in about 1 ns, which is several orders of magnitude faster than 0.5 ms required for the electron transfer from Q_A to Q_B[23,39]. Three plastoquinone exchange pathways were previously identified by molecular dynamic simulations of PSII[40]. One of these ensued close to the heme of cytochrome b559, and might coincide with the hydrophobic cavity that is described in this work. This part of the PSII hydrophobic cavity was exposed to the membrane, providing an ideal binding site (if one even exists) to the cytochrome b6f complex. Our suggested mechanism does not require an instantaneous escape of reduced Q_B, and the exchange of the reduced and oxidised plastoquinones might take place at the edge of the hydrophobic cavity, or even outside in the mid-membrane medium (Fig. 5).

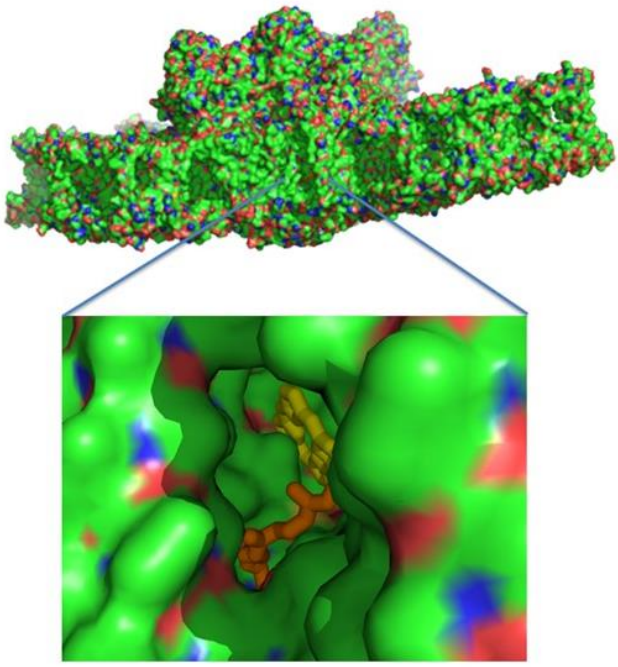

Figure 5: A surface presentation of PSII viewed from the membrane interior.

Zooming the middle reveilles; a hydrophobic cavity, where pheophytin A and part of the Q_B isoprenyl chain are apparent.

C. ohadii was far less sensitive to Diuron (DCMU) than other green algae[9]. This effect can be explained by the tighter binding of Q_B and reduced Diuron accessibility to its binding site. A recent study on the binding properties of the photosynthetic herbicides with the Q_B site of the D1 protein in plants have demonstrated that the high affinity inhibitors, such as Diuron, have replaced Q_B at its binding site [38-42]. A similar mode of interaction was established for Terbutryn binding in cyanobacterial PSII [43]. The less potent herbicides, such as Bentazon, bind away from this site in a manner that should prevent the secondary quinones from accessing the cavity, as proposed in this manuscript. Thus, a high metabolic rate, such as rapid lipid production, might serve as the best route to protect PSII from the damage that is caused by the intense illumination[34,44]. The accumulation of quinones in the vicinity of the reaction centre (CLA407/A), with Q_B and the heme of PsbF, might also provide an ideal environment for cycling the excess electrons, or to quench the radicals when they occur (Fig. 4c). This is in line with the suggestion that PsbL prevents the reduction of PSII by the back electron flow from plastoquinol and protecting PSII from photoinactivation, whereas PsbJ regulates the forward electron flow from Q_A^{*-} to the plastoquinone pool[2].

In conclusion, we reported the most complete description of a eukaryotic PSII cryoEM structure from the high-light resistant green algae *C. ohadii*, revealing a tight encapsulation and robust protection of the OEC, providing a structural basis for the algae's ability to resist photodamage, even at extreme illumination intensities. On the electron acceptor side, we identified a novel subunit Psb10 that together with PsbE, PsbF, and PsbY, shielded cytochrome b559 from its local environment. Finally, we detected the elusive Q_B in our structure, probably due to the unique architecture of its hydrophobic binding pocket in *C. ohadii* PSII, that leaves ample room for

additional quinones to occupy, thus generating a protective mechanism that prevent over-reduction of Q_B molecules.

Materials and Methods

Purification of the PSII supercomplex from the *C. ohadii* cells

The *C. ohadii* cells were cultured in 10 litres of TAP (Tris-Acetate-Phosphate) minimal medium under continuous white light (80 µE) at 25°C for about 4 days, until they reached an absorbance of 0.75 OD at 730 nm. The culture was harvested by centrifugation at 3,500 g for 5 min and resuspended in a medium containing 25 mM MES-KOH, pH=6.0, 200 mM sucrose, 10 mM NaCl, and 5 mM $MgCl_2$. The cells were washed once in the same buffer, spun down by centrifugation at 5,000 g for 5 min, and then suspended in a homogenization buffer containing 30 mM MES-NaOH, pH=6.0, 300 mM sucrose, and 0.2 mM EDTA-Na. Protease-inhibitor cocktail was added to the final concentrations of 1mM PMSF, 1 µM pepstatin, 60 µM bestatin, and 1mM benzamidine. The cells were disrupted by an Avestin® EmulsiFlex-C3 at 2,000 psi (two cycles), and the resulting suspension was immediately diluted twice with a buffer containing 20 mM MES-NaOH, pH=6.0, and 300 mM sucrose, to decrease the EDTA concentration. The unbroken cells and starch granules were removed by centrifugation at 12,000 g for 5 min, and the membranes in the supernatant were precipitated by centrifugation in a Ti70 rotor at 148,200 g for 40 minutes. The pellet was suspended in the buffer that contained 20 mM MES-NaOH, pH=6.0, and 300 mM sucrose, giving a Chl concentration of 2.0 mg/ml.

n-Decyl-α-D-Maltopyranoside (α-DM) and n-octyl β-D-glucopyranoside were added dropwise to a final concentration of 2.0% and 0.75%, respectively. After stirring at 4°C for 25 min, the insoluble material was removed by centrifugation at 20,800 g for 15 min. The supernatant was loaded on the sucrose gradients in an SW-60 rotor (≈640 µg of chlorophyll per tube). The gradient composition was 20-50% sucrose, 20 mM Mes-NaOH, pH 6.0, and 0.2% αDM, and this was centrifuged at 310,000 g for 14-16 h. The Extended Data Fig X (below) shows the distribution of

the green bands in the tubes and SDS-PAGE of the main bands. The band containing PSII was diluted 10-fold to reduce the sucrose, using 20 mM MES-NaOH, 6.0, and 0.1% α-DM to remove the sucrose, and concentrated using the centrifugal concentrator Vivaspin®6 (MWCO 100,000 PES membrane), to a final chlorophyll concentration of 2.9 mg/ml, with an oxygen evolution activity of 336 µmole O_2/mg chl/h.

CryoEM and the image processing.

Three µl of purified PSI at a concentration of 3 mg/ml was applied to the glow-discharged holey carbon grids (Cu QUANTIFOIL® R1.2/1.3), then vitrified using a Leica GP2 plunge freezer (2.5 s blot, 4°C, 100% humidity). The images were collected on a 300 kV FEI Titan Krios2 electron microscope (EMBL, Heidelberg, Germany). A Gatan K3 Summit detector was used in a counting mode at a magnification of 105,000 (yielding a pixel size of 0.64 Å), with a total dose of 50.6 e/Å^2. Thermo Fisher Scientific EPU software was used to collect a total of 21,341 images, which were dose fractionated into 40 movie frames, with defocus values ranging from 0.8 to 1.8 µm, at 0.1 µm increments. The collected frames were motion-corrected and dose-weighted using MotionCor2[58]. The contrast transfer function parameters were estimated using Ctffind-4.1[59]. A total of 734,768 particles were picked using reference-free picking in RELION-v.3[60]. The picked particles were processed for reference-free 2D averaging, resulting in 508,108 particles for the initial model building; both steps were performed when using RELION. Following the initial model creation, the 2D subset was used for the 3D classification, resulting in three distinct classes in RELION. From these, the best class was selected, which contained a total of 379,578 particles. These particles were pooled together and processed for 3D homogeneous refinement and postprocessing using RELION. The reported 2.34 Å resolution of PSII was based on a gold-standard refinement, applying the 0.143 criteria on the FSC between the reconstructed half-maps. (Extended Data Fig. 2 and Extended Data Table 2)

Data availability: The atomic coordinates of the three supercomplexes have been deposited in the Protein Data Bank, with accession code PDB 8BD3. The cryoEM maps have been deposited in the Electron Microscopy Data Bank, with accession codes PDB entry ID 8BD3 and EMDB entry ID EMD 15973

Acknowledgements: The authors thank the Electron Microscopy Core Facility (EMCF) at the European Molecular Biology Laboratory (EMBL) for their support. Dr Felix Weis is gratefully acknowledged and thanked for his excellent assistance and guidance in the data collection. The molecular graphics and analyses were performed with UCSF Chimera, which was developed by the Resource for Biocomputing, Visualization, and Informatics at the University of California, San Francisco, with support from NIH P41-GM103311. This work was supported by The Israel Science Foundation (Grant No. 199/21).

Author contributions: N.N. designed and preformed the experiments, organised the data collection, and built the structural model. M.F. designed and implemented the *C. ohadii* growth, the protein purifications, and purified the PSII complexes. D.K. processed the cryoEM data, calculated the results, and built the model. I.C. helped with the cryoEM calculation, and writing the manuscript.

Competing interests: The authors declare that there are no competing interests.

319 **Abbreviations:** Plastoquinone: dimethyl-1,4-benzoquinone molecule, with a side chain of nine
320 isoprenyl units (PQ); PQ, plastoquinone; Q_A and Q_B, primary and secondary quinone electron
321 acceptors; OEX, water oxidizing complex.
322

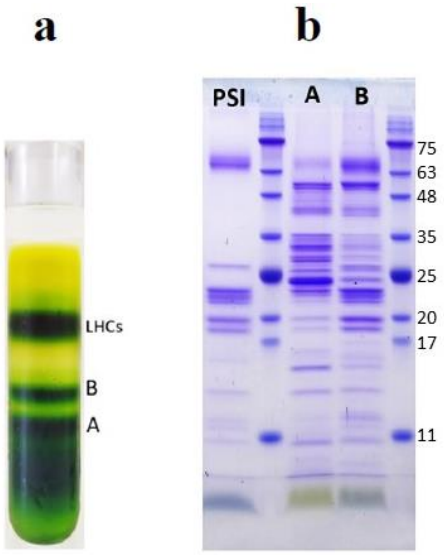

323

324 **Supplementary Figure 1**: **Sucrose gradient and SDS-PAGE of *Chlorella ohadii* PSII**
325 **preparation:**
326 **a.** Sucrose density gradient of the final *Chlorella ohadii* PSII preparation. The three fractions
327 collected are marked A, B, and LHCs. The A fraction was used for cryo-EM data collection. **b.**
328 SDS-PAGE of the fractions A and B and previous PSI preparation for comparison with new
329 preparation.
330

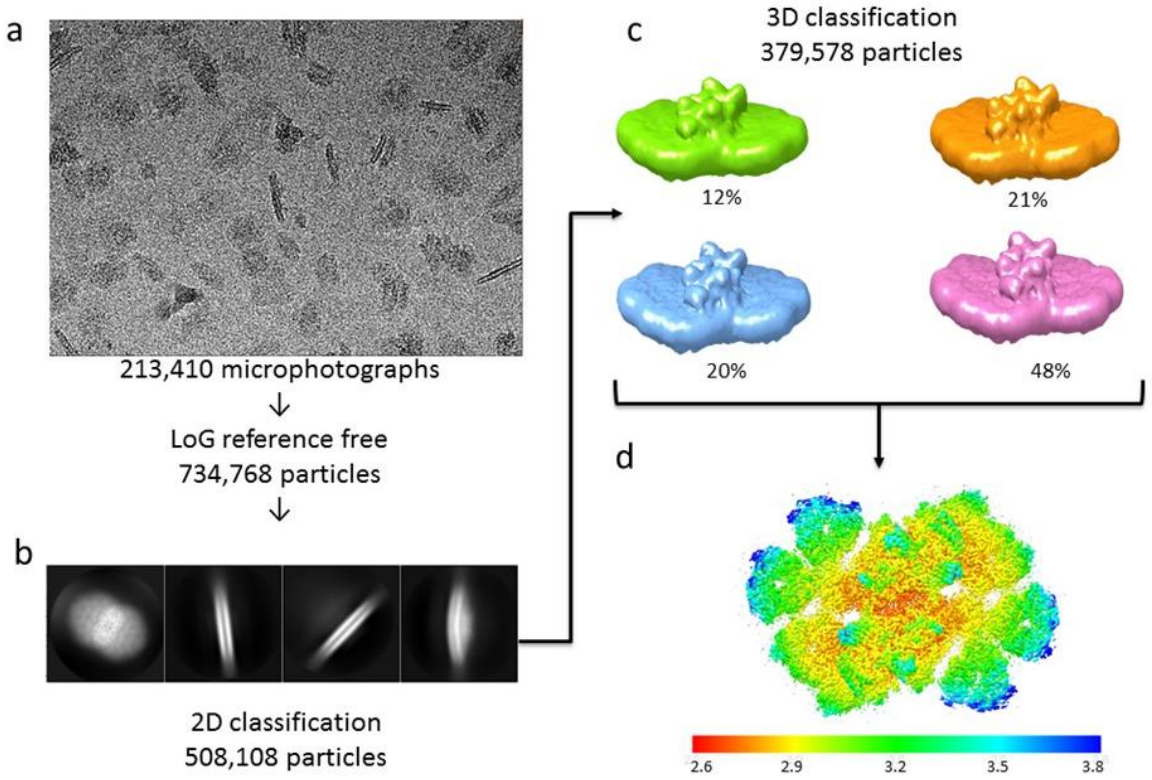

Supplementary Figure 2: **Cryo-EM data collection and processing scheme for unstacked PSII complex.**
a. Sample micrograph collected for the *Chlorella ohadii* PSII dataset displaying stacked and unstacked PSII particles from multiple views. **b.** 2D classes showing unstacked PSII complexes were created in RELION followed by 3D classification. **c.** Chosen unstacked PSII 3D classes subjected to refinement with numbers and percentage of all chosen particles. **d**. Final model of Chlorella ohadii PSII with a color-coded global resolution of 2.72 Å.

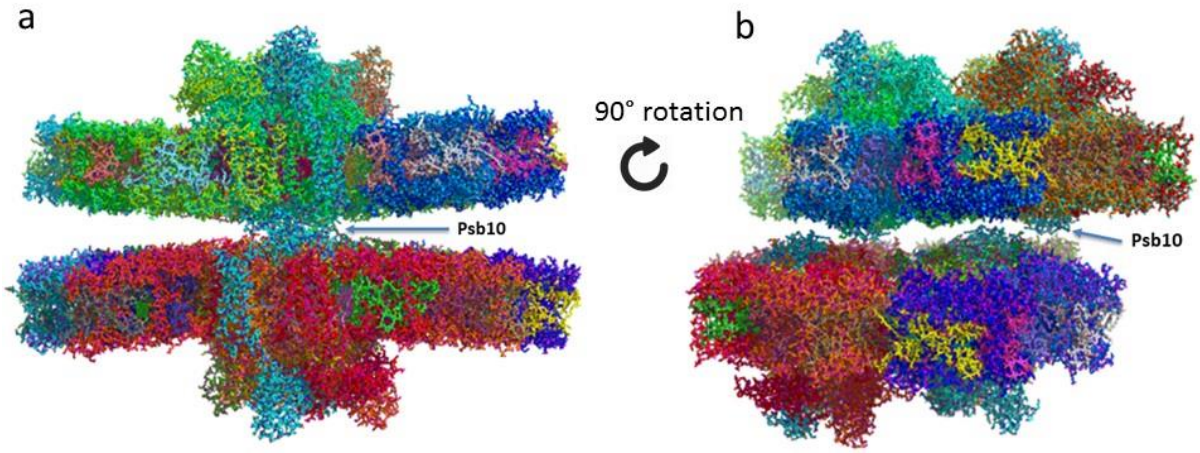

Supplementary Fig.3: Stacked PSII from *Chlorella ohadii* showing that Psb10 is involved in the stacking formation.

a. Side view along the membrane plane of stacked PSII. Psb10 may provide contacts for PSII dimer stacking. b. 90° rotation in the membrane plane of the complex presented on S.Fig.3a.

In the presented algae and another inferior plants present in PDB, we see 3-5 copies, whereas high plant contain mostly 1, sometime 2 copies.

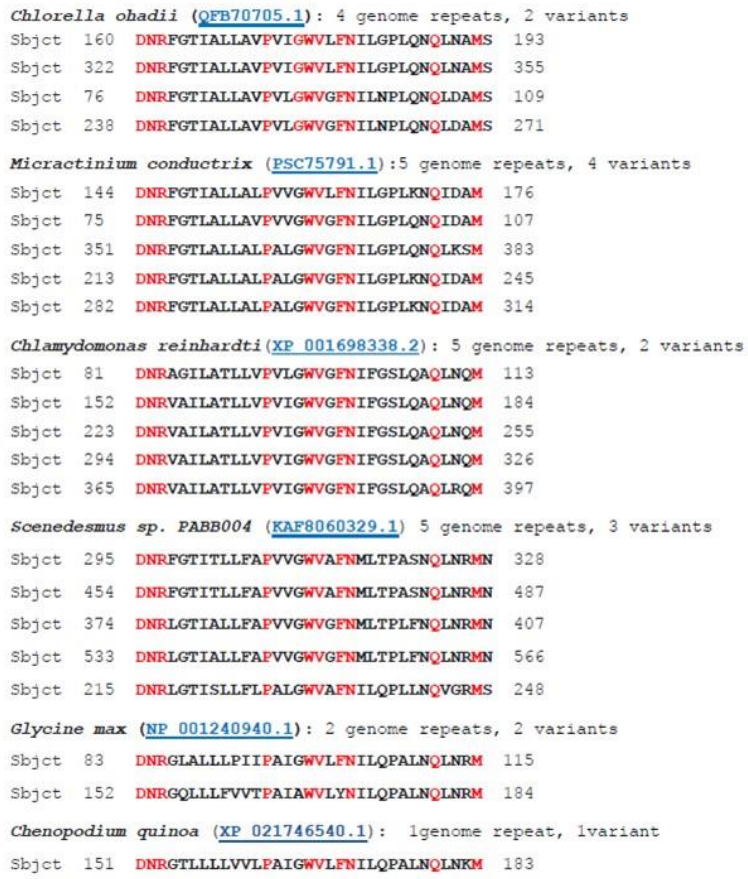

Supplementary Fig.4. Number of different copies of the PsbY, presented in the single transcripts of 4 algae and 2 high plants.

In the presented algae and another inferior plants present in PDB, we see 3-5 copies, whereas high plant contain mostly 1, sometime 2 copies.

References

1. Croce R. Light harvesting in oxygenic photosynthesis. Biochim Biophys Acta Bioenerg. 2020 Apr 1;1861(4):148172. doi: 10.1016/j.bbabio.2020.148172.

2. Yocum CF. (2022) Photosystem 2 and the oxygen evolving complex: a brief overview. Photosynthesis Research https://doi.org/10.1007/s11120-022-00910-1

3. Nelson, N. & Ben-Shem, A. The complex architecture of oxygenic photosynthesis. Nat. Rev. Mol. Cell Biol. 5, 971–982 (2004).

4. Sheng, X., Watanabe, A., Li, A., Kim, E., Song, C., Murata, K., Song, D., Minagawa, J., Liu, Z. Structural insight into light harvesting for photosystem II in green algae. Nat Plants 5: 1320-1330 (2019).

5. Drop, B. et al. Light-harvesting complex II (LHCII) and its supramolecular organization in Chlamydomonas reinhardtii. Biochim. Biophys. Acta 1837, 63–72 (2014).

6. Aro, E.-M., Virgin, I. & Andersson, B. Photoinhibition of Photosystem II. Inactivation, protein damage and turnover. *Biochimica et Biophysica Acta (BBA) - Bioenergetics* **1143**, 113-134, doi:https://doi.org/10.1016/0005-2728(93)90134-2 (1993)

7. Fischer, B. B., Hideg, É. & Krieger-Liszkay, A. Production, Detection, and Signaling of Singlet Oxygen in Photosynthetic Organisms. *Antioxidants & Redox Signaling* **18**, 2145-2162, doi:10.1089/ars.2012.5124 (2013).

8. Treves, H. et al. A newly isolated Chlorella sp. from desert sand crusts exhibits a unique resistance to excess light intensity. FEMS Microbiology Ecology 86, 373-380, doi:10.1111/1574-6941.12162 (2013)

9. Treves, H. *et al.* The mechanisms whereby the green alga Chlorella ohadii, isolated from desert soil crust, exhibits unparalleled photodamage resistance. *New Phytologist* **210**, 1229-1243, doi:10.1111/nph.13870 (2016).

10. Kedem, I., Milrad, Y., Kaplan, A. & Yacoby, I. Juggling Lightning: How Chlorella ohadii handles extreme energy inputs without damage. *Photosynthesis Research*, doi:10.1007/s11120-020-00809-9 (2021).

11. Ananyev, G., Gates, C., Kaplan, A. & Dismukes, G. C. Photosystem II-cyclic electron flow powers exceptional photoprotection and record growth in the microalga Chlorella ohadii. *Biochimica et Biophysica Acta (BBA) - Bioenergetics* **1858**, 873-883, doi:https://doi.org/10.1016/j.bbabio.2017.07.001 (2017).

12. Shen, L., Huang, Z., Chang, S., Wang, W., Wang, J., Kuang, T., Han, G., Shen, J.R., Zhang, X. Structure of a C2S2M2N2-type PSII-LHCII supercomplex from the green algaChlamydomonas reinhardtii. Proc Natl Acad Sci U S A 116: 21246-21255 (2019).

13. Bricker TM, Frankel LK.J Auxiliary functions of the PsbO, PsbP and PsbQ proteins of higher plant Photosystem II: a critical analysis. Photochem Photobiol B. 2011 Jul-Aug;104(1-2):165-78. doi: 10.1016/j.jphotobiol.2011.01.025.

14. Ettinger WF, Theg SM (1991) Physiologically active chloroplasts contain pools of unassembled extrinsic proteins of the photosynthetic oxygen evolving enzyme complex in the thylakoid lumen. J Cell Biol 115:321–328. https://doi.org/10.1083/jcb.115.2.321

15. Ifuku K, Yamamoto Y, Ono T-A, Usgugara SM, Sati F (2005) PsbP protein, but not PsbQ protein, is essential for the regulation and stabilization of photosystem II in higher plants. Plant Physiol 139:1175–1184. https://doi.org/10.1104/pp.105.068643

16. Bayro-Kaiser V. and Nelson N. Temperature Sensitive Photosynthesis: point mutated CEF-G, PRK or PsbO act as temperature-controlled switches for essential photosynthetic processes. Frontiers in Plant Science. 11:562985. doi: 10.3389/fpls.2020.562985 (2020).

17. Mayfield SP, Rahire M, Frank G, Zuber H, Rochaix JD. Expression of the nuclear gene encoding oxygen-evolving enhancer protein 2 is required for high levels of photosynthetic oxygen evolution in Chlamydomonas reinhardtii. Proc Natl Acad Sci U S A. 1987 Feb;84(3):749-53. doi: 10.1073/pnas.84.3.749.

18. Rochaix, J.-D. & Bassi, R. LHC-like proteins involved in stress responses and biogenesis/repair of the photosynthetic apparatus. *Biochemical Journal* **476**, 581-593, doi:10.1042/bcj20180718 (2019).

19. Liu, J., Lu, Y., Hua, W. & Last, R. L. A New Light on Photosystem II Maintenance in Oxygenic Photosynthesis. *Frontiers in Plant Science* **10**, doi:10.3389/fpls.2019.00975 (2019).

20. Caspy I, Fadeeva1 M, Mazor Y and Nathan Nelson N (2021) Structure of Dunaliella Photosystem II reveals conformational flexibility of stacked and unstacked supercomplexes. bioRxiv, DOI: 10.1101/2021.11.29.470333

21. Banerjee S, Seal S, Dey R, Mondal KK, Bhattacharjee P. Mutational spectra of SARS-CoV-2 orf1ab polyprotein and signature mutations in the United States of America. J Med Virol. 2021 Mar;93(3):1428-1435. doi: 10.1002/jmv.26417. Epub 2020 Aug 25.

22. Nelson, N. and Yocum, C. (2006). Structure and Function of Photosystems I and II. **Annu.** Rev. Plant Biol. 57, 521-565.

23. de Wijn R, van Gorkom HJ. Biochemistry. Kinetics of electron transfer from Q(a) to Q(b) in photosystem II. 2001 Oct 2;40(39):11912-22. doi: 10.1021/bi010852r.

24.Renger G, Light induced oxidative water splitting in photosynthesis: energetics, kinetics and mechanism, J. Photochem. Photobiol. B Biol. 104 (2011) 35–43.

25.Rappaport F, Guergova-Kuras M, Nixon PJ, Diner BA, Lavergne J. Kinetics and pathways of charge recombination in photosystem II, Biochemistry 41 (2002) 8518–8527.

26.Eisenstadt D, Barkan E, Luz B, Kaplan A. Enrichment of oxygen heavy isotopes during photosynthesis in phytoplankton, Photosynth. Res. 103 (2010) 97–103.

27. Müh F, Renger T, Zouni A. Crystal structure of cyanobacterial photosystem II at 3.0 Å resolution: a closer look at the antenna system and the small membrane- intrinsic subunits, Plant Physiol. Biochem. 46 (2008) 238–264.

28. P. Pospisil, Production of reactive oxygen species by photosystem II as a response to light and temperature stress. Front. Plant Sci. 7, 1950 (2016).

458
459 29. Fantuzzi A, Allgöwer F, Baker H, McGuire G, Teh WK, Gamiz-Hernandez AP, Kaila
460 VRI, Rutherford AW. Bicarbonate-controlled reduction of oxygen by the Q A semiquinone in
461 Photosystem II in membranes. Proc Natl Acad Sci U S A. 2022 Feb 8;119(6):e2116063119.
462 doi: 10.1073/pnas.2116063119.
463
464 30. Liu, J., Lu, Y., Hua, W. & Last, R. L. A New Light on Photosystem II Maintenance in
465 Oxygenic Photosynthesis. Frontiers in Plant Science 10, doi:10.3389/fpls.2019.00975 (2019).
466
467 31. Li, L., Aro, E.-M. & Millar, A. H. Mechanisms of Photodamage and Protein Turnover in
468 Photoinhibition. Trends in Plant Science 23, 667-676,
469 doi:https://doi.org/10.1016/j.tplants.2018.05.004 (2018).
470
471 32. Keren, N. & Krieger‐Liszkay, A. Photoinhibition: molecular mechanisms and
472 physiological significance. Physiologia Plantarum 142, 1-5 (2011).
473
474 33. Virtanen O, Khorobrykh S, Tyystjärvi E. Acclimation of Chlamydomonas reinhardtii .33
475 to extremely strong light. Photosynth Res. 2021 Jan;147(1):91-106. doi: 10.1007/s11120-020-
476 00802-2. Epub 2020 Dec
477
478 34. Røkke G, Melø TB, Hohmann-Marriott MF. The plastoquinone pool of Nannochloropsis
479 oceanica is not completely reduced during bright light pulses. PLoS One. 2017 Apr
480 .12;12(4):e0175184. doi: 10.1371/journal.pone.0175184. eCollection 2017
481
482 35. Suslichenko IS, Tikhonov AN. Photo-reducible plastoquinone pools in chloroplasts of
483 Tradescentia plants acclimated to high and low light. FEBS Lett. 2019 Apr;593(8):788-798. doi:
484 10.1002/1873-3468.13366. Epub 2019 Mar 30.PMID: 30896038
485
486 36. Guskov, A.; Kern, J.; Gabdulkhakov, A.; Broser, M.; Zouni, A.; Saenger, W. Cyanobacterial
487 photosystem II at 2.9 Å resolution: role of quinones, lipids, channels and chloride. Nat. Struct.
488 Mol. Biol., 2009, 16, 334-342.
489
490 37. Loll, B., Kern, J., Saenger, W., Zouni, A. & Biesiadka, J. Towards complete cofactor
491 arrangement in the 3.0 A˚resolution structure of photosystem II. Nature 438, 1040–1044 (2005).
492
493 38. Lambreva MD, Russo D, Polticelli F, Scognamiglio V, Antonacci A, Zobnina V, Campi G,
494 Rea G. Structure/Function/Dynamics of Photosystem II Plastoquinone Binding Sites. Curr Protein
495 Pept Sci. 2014;15(4):285-95. doi: 10.2174/1389203715666140327104802.
496
497 39. Moser CC, et al. Nature of biological electron transfer. Nature 355(6363):796-802. doi:
498 10.1038/355796a0. 1992. PMID: 1311417
499
500 40. Van Eerden FJ, Melo MN, Frederix PWJM, Periole X, Marrink SJ. Nat Commun. Exchange
501 pathways of plastoquinone and plastoquinol in the photosystem II complex
502 2017 May 10;8:15214. doi: 10.1038/ncomms15214.
503
504 41. Battaglino B, Grinzato A, Pagliano C. Plants (Basel). Binding Properties of Photosynthetic
505 Herbicides with the Q B Site of the D1 Protein in Plant Photosystem II: A Combined Functional
506 and Molecular Docking Study. 2021 Jul 21;10(8):1501. doi: 10.3390/plants10081501
507

42. Erickson JM, Rahire M, Bennoun P, Delepelaire P, Diner B, Rochaix J. Herbicide resistance in Chlamydomonas reinhardtii results from a mutation in the chloroplast gene for the 32-kilodalton protein of photosystem II. Proc Natl Acad Sci U S A. 1984 Jun;81(12):3617-21. doi: 10.1073/pnas.81.12.3617

43. Broser et al., Structural basis of cyanobacterial photosystem II Inhibition by the herbicide terbutryn. J Biol Chem. 2011 May 6;286(18):15964-72. doi: 10.1074/jbc.M110.215970.

44. Vass, I. Molecular mechanisms of photodamage in the Photosystem II complex. Biochimica et Biophysica Acta (BBA) - Bioenergetics 1817, 209-217Zheng, S. Q. et al. MotionCor2: anisotropic correction of beam-induced motion for improved cryo-electron microscopy. Nat. Methods 14, 331–332 (2017).

45. Rohou, A. & Grigorieff, N. CTFFIND4: fast and accurate defocus estimation from electron micrographs. J. Struct. Biol. 192, 216–221 (2015).

46. Zivanov, J. et al. New tools for automated high-resolution cryo-EM structure determination in RELION-3. Elife 7, e42166 (2018).

47. Eldar, A., Landa, B. & Shkolnisky, Y. KLT picker: particle picking using data-driven optimal templates. J. Struct. Biol. 210, 107473 (2020).

48. Greenberg, I. & Shkolnisky, Y. Common lines modeling for reference free ab-initio reconstruction in cryo-EM. J. Struct. Biol. 200, 106–117 (2017).

49. Tang, G. et al. EMAN2: an extensible image processing suite for electron microscopy. J. Struct. Biol. 157, 38–46 (2007).

50. Badura, A. et al. Photo-induced electron transfer between photosystem 2 via cross-linked redox hydrogels. Electroanalysis 20, 1043–1047 (2008).